Available online at www.sciencedirect.com
ScienceDirect
Int. J. Electron. Commun. (AEÜ) 63 (2009) 728–735
International Journal AEÜ of Electronics and Communications
www.elsevier.de/aeue

Some useful properties of cross-Ψ_B-energy operator

Abdel-Ouahab Boudraa[a,b,*], Salem Benramdane[a], Jean-Christophe Cexus[b], Thierry Chonavel[c]

[a] *IRENav, Ecole Navale, Lanvéoc Poulmic, BP600, 29240 Brest-Armées, France*
[b] *E^3I^2, EA 3876, ENSIETA, 2 rue François Verny, 29806 Brest Cedex 09, France*
[c] *SC Department, ENST-Bretagne, B.P. 832, 29285 Brest, France*

Received 16 June 2007; accepted 28 May 2008

Abstract

In this paper, some useful properties of cross-Ψ_B-energy operator, which measures the interaction between two signals, are provided. We show that Ψ_B is a generalization of some extensions of Teager–Kaiser operator to complex signals. Due to its bilinearity, Ψ_B satisfies the quadratic superposition principle. We point out the link between the Ψ_B and the Lie bracket, which measures the instantaneous differences in the relative change between two signals. We show how the Ψ_B operator can handle wideband signals using bandpass filtering. We also show how the quadratic superposition law can be used for detection purpose.

Keywords: Cross-Ψ_B-energy operator; Teager energy operator; Complex valued-signals; Bandpass signals

1. Introduction

Cross Teager–Kaiser operator (CTKO) has been introduced by Kaiser [1], with a view to measure the interaction between two real signals x and y,

$$\Psi(x, y) = \dot{x}\dot{y} - x\ddot{y}. \tag{1}$$

This function is based on the Teager–Kaiser operator (TKO), which is a versatile tool for measuring instantaneous changes in sinusoidal energy. It represents the energy of the signal within a typical frequency band [1]. Ψ operator or CTKO has been extended to deal with complex-valued signals [2], yielding a new operator denoted by $\Psi_{\mathbb{C}}$ and defined by

$$\Psi_{\mathbb{C}}(x, y) = 0.5[\dot{x}^*\dot{y} + \dot{x}\dot{y}^*] - 0.5[x\ddot{y}^* + x^*\ddot{y}], \tag{2}$$

where x and y are two complex-valued signals and x^* and y^* their respective conjugates. A positive symmetric modification of $\Psi_{\mathbb{C}}$, denoted Ψ_B, has also been proposed in [2], where

$$\begin{aligned}\Psi_B(x, y) &= 0.5[\Psi_{\mathbb{C}}(x, y) + \Psi_{\mathbb{C}}(y, x)]\\ \Psi_B(x, y) &= [0.5\dot{x}\dot{y}^* - 0.25(\ddot{x}y^* + x\ddot{y}^*)]\\ &\quad + [0.5\dot{x}^*\dot{y} - 0.25(\ddot{x}^*y + x^*\ddot{y})].\end{aligned} \tag{3}$$

The link between Ψ_B operator and the cross-Wigner–Ville distribution shows that Ψ_B is well suited to study non-stationary signals [2] and that time-delay estimation between two signals x and y can be addressed via the interaction measure $\Psi_B(x, y)$ [3]. We have also shown how Ψ_B can be used for functional segmentation of dynamic nuclear cardiac images [4], time delay estimation [5] or time series analysis [6].

The paper is organized as follows. In Section 2 we show that different energy operators, based on the TKO, recently introduced in the literature can be derived from Ψ_B operator. Formulation of Ψ_B operator using analytic signals is presented in Section 3. The link between Ψ_B operator and the

* Corresponding author at: IRENav, Ecole Navale, Lanvéoc Poulmic, BP600, 29240 Brest-Armées, France. Tel.: +33 2 98 23 40 44; fax: +33 2 98 23 38 57.
E-mail address: boudra@ecole-navale.fr (A.-O. Boudraa).

1434-8411/$ - see front matter © 2008 Elsevier GmbH. All rights reserved.
doi:10.1016/j.aeue.2008.05.014

Lie bracket is established in Section 4. Due to its bilinearity, we show in Section 5 that Ψ_B satisfies the quadratic superposition principle. Chain rule properties of Ψ_B are introduced in Section 6. In Section 7 we show how the quadratic principle verified by Ψ_B can be usedas a strategy for transients detection. Simulation results are presented in Section 8 and concluding remarks are provided in Section 9.

2. TKO-based energy operators

We show that some energy operators based on the TKO [7,8], recently introduced in the literature are particular cases of Ψ_B operator. We note that the first term of the right-hand side of Eq. (3) corresponds to Teager cross-correlation (TCC) between x and y introduced by Bysted et al. [7]. The second term is the conjugate of the first one. Thus, Ψ_B may be viewed as a generalization of TCC. The TKO has been first extended to cover complex signals by Maragos and Bovik [9] as

$$\Psi_{\mathbb{C}_1}(x) = \|\dot{x}\|^2 - \mathrm{Re}[x^*\ddot{x}] \tag{4}$$

and by Hamila et al. [8] as

$$\Psi_{\mathbb{C}_2}(x) = \dot{x}\dot{x}^* - 0.5[\ddot{x}x^* + x\ddot{x}^*]. \tag{5}$$

If $x = y$, thus $\Psi_{\mathbb{C}}(x, y) = \Psi_{\mathbb{C}_2}(x) \Rightarrow \Psi_B(x, y) = 0.5[\Psi_{\mathbb{C}}(x, y) + \Psi_{\mathbb{C}}(y, x)] = \Psi_{\mathbb{C}_2}(x)$. Furthermore, letting $x = y$ in Eq. (3) yields $\Psi_B(x, y) = \dot{x}^*\dot{x} - 0.5[x\ddot{x}^* + x^*\ddot{x}] = \Psi_{\mathbb{C}_1}(x)$. Thus, $\Psi_{\mathbb{C}_1}$ and $\Psi_{\mathbb{C}_2}$ are particular cases of Ψ_B. In what follows, $\Psi_B(x, x)$ will be denoted simply by $\Psi_B(x)$. In addition, letting $x(t) = x_r(t) + \mathrm{j}x_i(t)$ and $y(t) = y_r(t) + \mathrm{j}y_i(t)$ denote the decomposition of x and y into real and imaginary parts ($\mathrm{j}^2 = -1$)

$$\Psi_B(x, y) = \Psi_B(x_r, y_r) + \Psi_B(x_i, y_i). \tag{6}$$

Eq. (6) clearly shows that Ψ_B is real valued function, as expected for an energy operator.

3. Expression of Ψ_B using analytic signals

Complex signals are used in various areas of signal processing. In the continuous-time domain, they appear, for example, in the description of narrowband signals. Indeed, the appropriate definition of instantaneous phase or amplitude of such signals requires the introduction of the analytic signal, which is necessarily complex. Let x and y be two real signals, and x_A and y_A, respectively, their corresponding analytic signals: $x_A = x + \mathrm{j}\mathscr{H}(x)$ and $y_A = y + j\mathscr{H}(y)$, where $\mathscr{H}(\cdot)$ is the Hilbert transform. The cross-energy $\Psi_B(x_A, y_A)$ can be directly expressed in terms of x, y, $\mathscr{H}(x)$ and $\mathscr{H}(y)$.

Proposition 1.

$$\Psi_B(x_A, y_A) = [\dot{x}\dot{y} - 0.5(x\ddot{y} + y\ddot{x})] + \dot{\mathscr{H}}(x)\dot{\mathscr{H}}(y) - 0.5[\mathscr{H}(x)\ddot{\mathscr{H}}(y) + \mathscr{H}(y)\ddot{\mathscr{H}}(x)]. \tag{7}$$

Proof.

$$\dot{x}_A^*\dot{y}_A + \dot{x}_A\dot{y}_A^* = 2\dot{x}\dot{y} + 2\dot{\mathscr{H}}(x)\dot{\mathscr{H}}(y)$$
$$x_A\ddot{y}_A^* + x_A^*\ddot{y}_A = 2x\ddot{y} + 2\mathscr{H}(x)\ddot{\mathscr{H}}(y)$$
$$\ddot{x}_A^*y_A + \ddot{x}_Ay_A^* = 2\ddot{x}y + 2\mathscr{H}(y)\ddot{\mathscr{H}}(x).$$

Using Eq. (3) we obtain

$$\Psi_B(x_A, y_A) = [\dot{x}\dot{y} - 0.5(x\ddot{y} + y\ddot{x})] + \dot{\mathscr{H}}(x)\dot{\mathscr{H}}(y) - 0.5[\mathscr{H}(x)\ddot{\mathscr{H}}(y) + \mathscr{H}(y)\ddot{\mathscr{H}}(x)]. \tag{8}$$

It is easy to see that

$$\dot{x}\dot{y} - 0.5(x\ddot{y} + y\ddot{x}) = 2\dot{x}\dot{y} - 0.5\frac{\mathrm{d}^2xy}{\mathrm{d}t^2}, \tag{9}$$

$$-0.5[\mathscr{H}(x)\ddot{\mathscr{H}}(y) + \mathscr{H}(y)\ddot{\mathscr{H}}(x)] = -0.5\frac{\mathrm{d}^2\mathscr{H}(x)\mathscr{H}(y)}{\mathrm{d}t^2} + \dot{\mathscr{H}}(x)\dot{\mathscr{H}}(y). \tag{10}$$

Inserting (9) and (10) in (8) completes the proof.

4. Ψ_B operator and the Lie bracket

The Lie bracket can be used to measure the instantaneous differences in the relative change between real signals x and y [10] and is defined by

$$\mathrm{L}[x, y] = \dot{x}y - x\dot{y}. \tag{11}$$

Clearly, from Eqs. (1) and (11) we have $\Psi(x, y) = \mathrm{L}[x, \dot{y}]$, and for $y = \dot{x}$, $\mathrm{L}[x, y]$ becomes the continuous-time TKO [1]: $\Psi(x) = \dot{x}^2 - x\ddot{x}$, which has been used for tracking the energy of a source producing an oscillation [1] and for signal and speech AM–FM demodulation [11]. In general, if x and y represent displacements in some generalized motions, $\Psi(x, y) = \mathrm{L}[x, \dot{y}] = \dot{x}\dot{y} - x\ddot{y}$ has dimension of an energy (per unit mass), and hence it may be viewed as the cross-energy between x and y. Furthermore, considering complex signals with Ψ_B operator, the link between Ψ_B and Lie bracket can be expressed by the following proposition.

Proposition 2. *Ψ_B operator is related to Lie bracket by*

$$\Psi_B(x, y) = 0.5[\mathrm{L}(x_r, \dot{y}_r) + \mathrm{L}(x_i, \dot{y}_i) - \mathrm{L}(\dot{x}_r, y_r) - \mathrm{L}(\dot{x}_i, y_i)]. \tag{12}$$

Proof.

$$\begin{aligned}\Psi_B(x, y) &= 0.25[\Psi(x, y^*) + \Psi(x^*, y) + \Psi(y, x^*) + \Psi(y^*, x)] \\ &= 0.25[\mathrm{L}(x, \dot{y}^*) + \mathrm{L}(x^*, \dot{y}) + \mathrm{L}(y, \dot{x}^*) + \mathrm{L}(y^*, \dot{x})].\end{aligned} \tag{13}$$

In addition, we clearly have $\mathrm{L}(u, \dot{v}^*) + \mathrm{L}(u^*, \dot{v}) = 2[\mathrm{L}(u_r, \dot{v}_r) + \mathrm{L}(u_i, \dot{v}_i)]$ and $\mathrm{L}(u, v) = -\mathrm{L}(v, u)$, which completes the proof. Eq. (12) shows that Ψ_B operator is a weighted sum of cross-energy terms, $\mathrm{L}[\ldots]$, and thus it confirms that Ψ_B is a measure of cross-energy between x and y.

5. Quadratic superposition principle

It is straightforward to see that Ψ_{B} is a bilinear symmetric operator on the vectorial space of complex signals defined on $\mathbb{R}$. In other words we have

$$\Psi_{\mathrm{B}}(x, y) = \Psi_{\mathrm{B}}(y, x), \tag{14}$$

$$\Psi_{\mathrm{B}}(x_1 + x_2, y) = \Psi_{\mathrm{B}}(x_1, y) + \Psi_{\mathrm{B}}(x_2, y), \tag{15}$$

$$\forall a, b \in \mathbb{R} \quad \Psi_{\mathrm{B}}(ax, by) = ab\Psi_{\mathrm{B}}(x, y). \tag{16}$$

Relation (16) shows that the Ψ_{B} of two signals is proportional to Ψ_{B} of their scaled versions. This implies that Ψ_{B} is robust to amplitude scaling. Eqs. (14)–(16) are clearly desirable properties for a cross-energy operator. Consider a signal consisting of K complex components $x_k(t)$ with real coefficients, c_k, $k \in \mathbb{N}$:

$$x(t) = \sum_{k=1}^{K} c_k x_k(t). \tag{17}$$

As a direct consequence, we have

$$\Psi_{\mathrm{B}}(x(t), x(t)) = \Psi_{\mathrm{B}}(x(t)) = \sum_{k,l=1}^{K} c_k c_l \Psi_{\mathrm{B}}(x_k, x_l). \tag{18}$$

In this expression, the K indexed terms $\Psi_{\mathrm{B}}(x_k)$ measure the energy of the indexed signals x_k while the $K(K-1)$ cross-terms measure the interaction between the different components. According to Eq. (18), Ψ_{B} of a K-component signal consists of K signal terms and $K(K-1)$ Ψ_{B} cross-terms. These terms measure the interaction between the different components of the signal. While the number of signal terms grows linearly with K, the number of cross-$\Psi_{\mathrm{B}}(x_k)$ terms grows quadratically with K.

For complex valued coefficients $\alpha, \beta \in \mathbb{C}$, the expression of $\Psi_{\mathrm{B}}(\alpha x, \beta y)$ is slightly more complicated. To describe it, let us introduce the following notation:

$$\tilde{\Psi}_{\mathrm{B}}(x, y) = \Psi_{\mathrm{B}}(x_r, y_i) - \Psi_{\mathrm{B}}(x_i, y_r). \tag{19}$$

Then, we have the following result:

$$\Psi_{\mathrm{B}}(\alpha x, \beta y) = \mathrm{Re}(\alpha\beta^*)\Psi_{\mathrm{B}}(x, y) + \mathrm{Im}(\alpha\beta^*)\tilde{\Psi}_{\mathrm{B}}(x, y). \tag{20}$$

This can be checked readily since from Eq. (6) we have

$$\begin{aligned}\Psi_{\mathrm{B}}(\alpha x, \beta y) &= \Psi_{\mathrm{B}}(\alpha_r x_r - \alpha_i x_i, \beta_r y_r - \beta_i y_i) \\ &\quad + \Psi_{\mathrm{B}}(\alpha_r x_i + \alpha_i x_r, \beta_r y_i + \beta_i y_r) \\ &= (\alpha_r\beta_r + \alpha_i\beta_i)[\Psi_{\mathrm{B}}(x_r, y_r) + \Psi_{\mathrm{B}}(x_i, y_i)] \\ &\quad + (\alpha_i\beta_r - \alpha_r\beta_i)[\Psi_{\mathrm{B}}(x_r, y_i) \\ &\quad - \Psi_{\mathrm{B}}(x_i, y_r)].\end{aligned} \tag{21}$$

Most often, complex signals arise from analytic representations, as mentioned above. In such situations, if x and y are real valued, then, for their analytic representations the value of $\tilde{\Psi}_{\mathrm{B}}$ is given by

$$\tilde{\Psi}_{\mathrm{B}}(x_{\mathrm{A}}, y_{\mathrm{A}}) = \Psi_{\mathrm{B}}(x, \mathscr{H}(y)) - \Psi_{\mathrm{B}}(\mathscr{H}(x), y). \tag{22}$$

6. Chain rule properties of Ψ_{B}

6.1. Derivative

Proposition 3. *The nth time derivative of $\Psi_{\mathrm{B}}(x, y)$ is given by*

$$[\Psi_{\mathrm{B}}(x, y)]^{(n)} = \sum_{k=0}^{n} C_n^k \Psi_{\mathrm{B}}(x^{(k)}, y^{(n-k)}). \tag{23}$$

Proof. The property clearly holds for $n = 1$:

$$[\Psi_{\mathrm{B}}(x, y)]^{(1)} = \Psi_{\mathrm{B}}(x, \dot{y}) + \Psi_{\mathrm{B}}(\dot{x}, y) \tag{24}$$

and the proof can be obtained by induction. In fact this only relies on the bilinearity property of Ψ_{B}. For instance, for the bilinear operator $\langle x, y\rangle = xy$, the well-known Leibniz derivation chain rule is given by

$$\langle x, y\rangle^{(n)} = \sum_{k=0,n} C_n^k x^{(k)} y^{(n-k)} \tag{25}$$

$$= \sum_{k=0,n} C_n^k \langle x^{(k)}, y^{(n-k)}\rangle. \tag{26}$$

In the same way, we get Eq. (23).

6.2. Integration

The cross-Ψ_{B}-energy of the integral of two signals, f and g, is given by

$$\begin{aligned}&\Psi_{\mathrm{B}}\left(\int_0^t f\,\mathrm{d}t', \int_0^t g\,\mathrm{d}t'\right) \\ &= 0.5[f^* g + f g^*] \\ &\quad - 0.25\left[\dot{g}^* \int_0^t f\,\mathrm{d}t' + \dot{g} \int_0^t f^*\,\mathrm{d}t'\right. \\ &\quad \left. + \dot{f}^* \int_0^t g\,\mathrm{d}t' + \dot{f} \int_0^t g^*\,\mathrm{d}t'\right].\end{aligned} \tag{27}$$

6.3. Composition

Consider the general situation where the signals f and g are function of second signals x and y, respectively, i.e. find $\Psi_{\mathrm{B}}(f, g)$. The result is

$$\begin{aligned}&\Psi_{\mathrm{B}}(f(x(t)), g(y(t))) \\ &= 0.5[\dot{x}^*\dot{y}\dot{g}(x)^*\dot{h}(y) + \dot{x}\dot{y}^*\dot{g}(x)\dot{h}(y)^*] - 0.25[g(x)(\ddot{y}\dot{h}(y) \\ &\quad + \dot{y}^2\ddot{h}(y))^* + g(x)^*(\ddot{y}\dot{h}(y) + \dot{y}^2\ddot{h}(y)) \\ &\quad + h(y)(\ddot{x}\dot{g}(x) + \dot{x}^2\ddot{g}(x))^* + h(y)^*(\ddot{x}\dot{g}(x) + \dot{x}^2\ddot{g}(x))].\end{aligned} \tag{28}$$

6.4. Filtering

We provide another property of practical importance, when dealing with wideband signals, that arises from the bilinearity of Ψ_{B}. Indeed, Ψ_{B} cannot handle wideband

signals and thus a bandpass filtering is required. Let x and y be two wideband signals and u and v the corresponding bandpass filtered ones defined as $u = x \star g$ and $v = y \star h$ where "$\star$" denotes convolution and g and h are the impulse responses of bandpass filters used.

Proposition 4. *The output of Ψ_B acting on the bandpass filtered signals u and v is given by*

$$\begin{aligned}\Psi_B(u, v) = {} & 0.5[(g^{(1)} \star x)^*(h^{(1)} \star y) + (g^{(1)} \star x)(h^{(1)} \star y)^*] \\ & - 0.25[(g \star x)(h^{(2)} \star y)^* + (g \star x)^*(h^{(2)} \star y) \\ & + (h \star y)(g^{(2)} \star x)^* + (h \star y)^*(g^{(2)} \star x))]. \end{aligned} \quad (29)$$

Proof. Since convolution commutes with time-differentiation, $(u \star v)^{(k)} = u \star v^{(k)}$, we can derive for u and v closed-form for the derivatives (Eq. (3)) that involve only the first and the second derivatives of the filters g and h. Finally, using the same development as in [12,13] Eq. (29) can be easily deduced. The advantage of Eq. (29) is that applying directly the derivation operators on the filters rather than on the signals themselves avoids one-sample discrete-time approximations of the derivatives that are, in general, sensitive to noise.

7. Detection strategy

We show how the quadratic superposition principle (Eq. (18)) verified by $\Psi_B$can be used for the detection of transients in noisy signals. This problem finds application in many fields of interest. To this end, we use the Ψ_B operator as a detector. In this paper, we limit ourselves to the problem of transient signals detection in the presence of AM–FM signals. Let us suppose that the observed signal is given by

$$s_i(t) = x(t) + y_i(t), \quad i \in \{1, 2\}, \quad (30)$$

where $x(t)$ is an AM–FM signal of interest given by

$$x(t) = a(t)\cos(\theta(t)) \quad (31)$$

and $y_i(t)$ is a transient signal. According to Eq. (18), we get

$$\begin{aligned}\Psi_B(s_i(t)) = {} & \Psi_B(x(t)) + \Psi_B(y_i(t)) \\ & + 2\Psi_B(x(t), y_i(t)). \end{aligned} \quad (32)$$

Based on the TKO [1], Ψ_B slowly tracks the AM and FM components of $s_i(t)$. When there is no transient present

$$y_i(t) = 0 \Rightarrow \Psi_B(s_i(t)) = a^2(t)\omega^2(t), \quad (33)$$

with $\omega(t) = \mathrm{d}\theta(t)/\mathrm{d}t$ [11]. If the signal $y_i(t)$ is present, Ψ_B output will deviate from $a^2(t)\omega^2(t)$. This is obvious from the instantaneous property of Ψ_B. Signal $y_i(t)$ can be detected by measuring the deviation, or error, $e_i(t)$ in the Ψ_B output:

$$\begin{aligned} e_i(t) &= \Psi_B(s_i(t) - x(t)) \\ &= \Psi_B(s_i(t)) + \Psi_B(x(t)) - 2\Psi_B(s_i(t), x(t)). \end{aligned} \quad (34)$$

8. Simulation results

The purpose of this section is to present applications of the introduced properties. We provide simulation results of Eqs. (7), (18) and (29).

8.1. Interaction measure

Application of Eq. (7) to measure the interaction between two signals is illustrated by Figs. 1 and 2. Two linear FM signals, $s_1(t)$ and $s_2(t)$, are shown in Figs. 1(b) and (c), respectively. The interaction measures using Ψ_B and cross-correlation (CC) are performed using a sliding window analysis of size T. Different T values, ranging from 3 to 71, have been tested. We found globally the same results. The presented results are obtained with T set to 17. The normalized value of $\Psi_B(s_1(t), s_2(t))$, calculated inside the window, is noted $I(t)$ (Fig. 1(e)). The instantaneous frequency (IF) of $s_2(t)$ increases linearly with time, while that of $s_1(t)$ decreases with time. The IF of signals $s_1(t)$ and $s_1(t)$ cross at point $Q(t = 126)$ (Fig. 1(a)). Interaction results of Ψ_B and

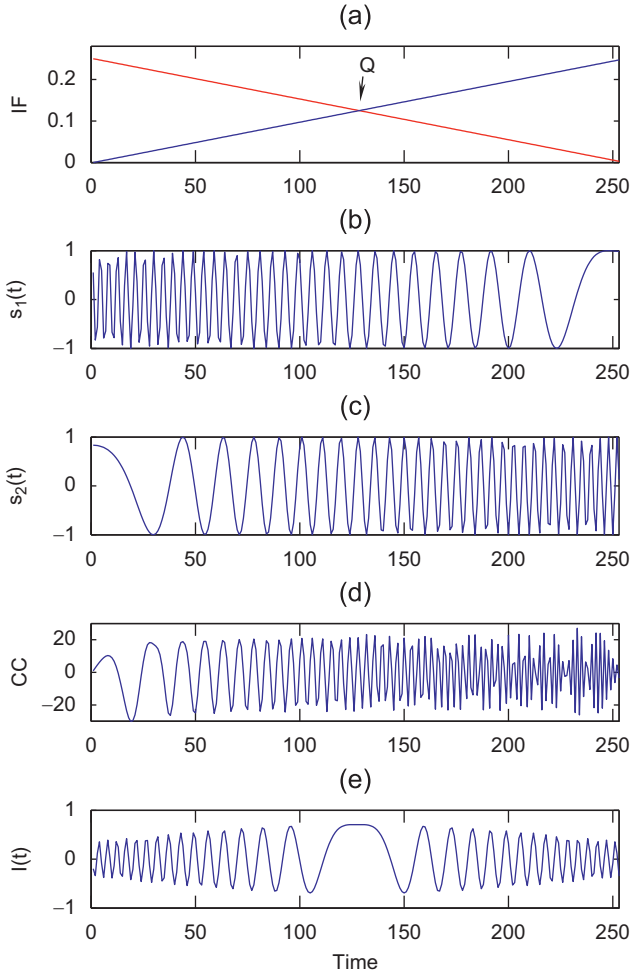

Fig. 1. Interaction measure using Ψ_B and CC: (a) Linear FM signals. (b) Signal $s_1(t)$. (c) Signal $s_2(t)$. (d) CC with a sliding window analysis. (e) Ψ_B with a sliding window analysis.

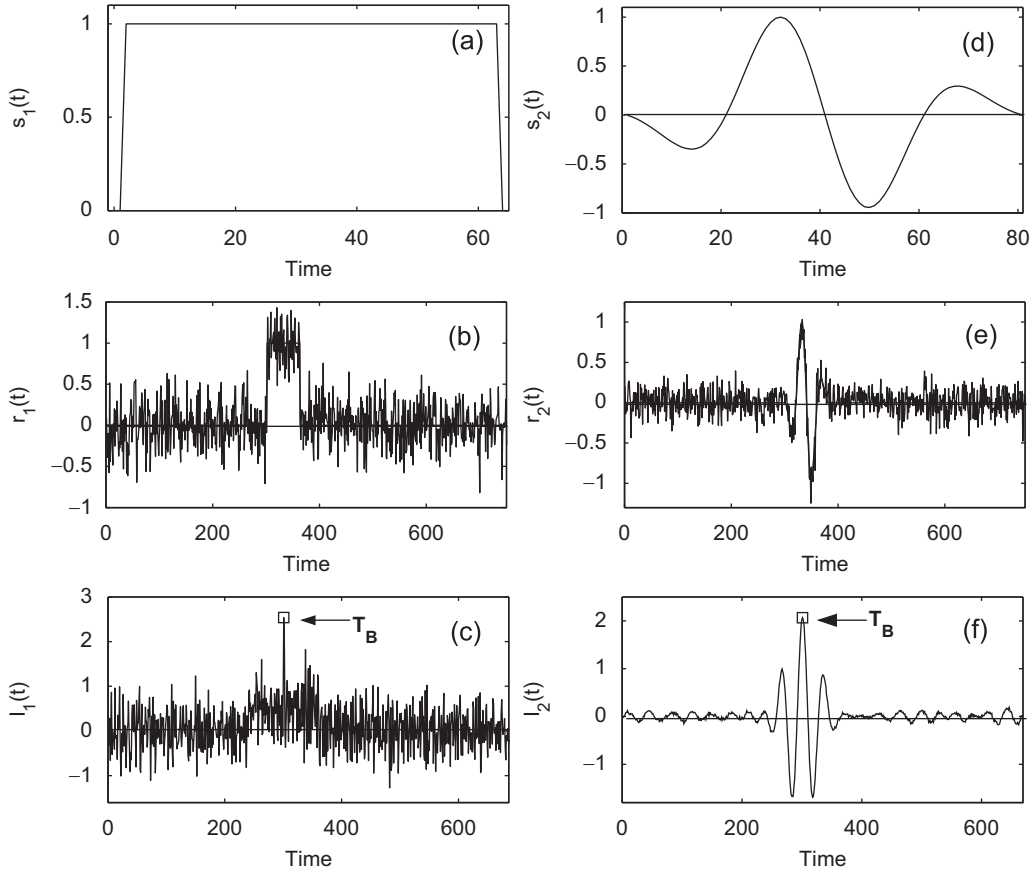

Fig. 2. Interaction measure using Ψ_B of signals of non-equal length.

CC are shown in Figs. 1(d) and (e), respectively. The maximum of interaction corresponding to the instant where the two IFs intercept (Q) is pointed out at $t = 126$ by Ψ_B (Fig. 1(e)). Away from the point Q, the amplitude of interaction decreases because there is less similarity or interaction between signals. As the IFs converge from the time origin to the their intersection, the interaction intensity of the signals increases and the maximum of interaction is achieved at the intersection (Fig. 1(e)). The CC measure fails to point out the maximum of interaction at Q and shows a maximum of interaction at $t = 233$ (Fig. 1(d)). Furthermore, as the IFs converge to Q or diverge from Q the CC measure does no yield clear interpretation and thus the interaction study of nonstationary signals is difficult.

Another example of application of Eq. (7) is shown in Fig. 2. Two synthetic signals, $s_1(t)$ and $s_2(t)$, of non-equal lengths with window size observation T of 65 and 81, respectively, are shown in Figs. 2(a) and (d). These signals, are time-shifted by 300 samples, corrupted by additive Gaussian noise and modified in amplitude by an attenuation coefficient of 0.7. The obtained signals $r_1(t)$ and $r_2(t)$ are shown in Figs. 2(b) and (e), respectively. For both $r_1(t)$ and $r_2(t)$ an interaction measure would show, in theory, a maximum of interaction located at $t = 300$. We use the smallest length signal as a sliding window and calculate the normalized Ψ_B, inside this window, between two signals of the same length $\Psi_B(I_1(t), I_2(t))$. Outputs of $\Psi_B$are shown in Figs. 2(c) and (f), indicating a net maximum at $t = T_B$. As expected both $\Psi_B(s_1(t), r_1(t))$ and $\Psi_B(s_2(t), r_2(t))$ peak to $T_B = 300$. Table 1 lists the T_B values calculated for $\Psi_B(s_1(t), r_1(t))$ and $\Psi_B(s_2(t), r_2(t))$ for different SNRs ranging from -6 to 9 dB. Each value of Table 1 corresponds to the average of an ensemble of 25 trials of T_B estimation. These results show that the performances of $\Psi_B$are very close to that of the theory and also that Ψ_B works correctly for moderately noisy signals.

8.2. Detection of transients

We show how the quadratic superposition principle (Eq. (18) and the filtering property (Eq. (29)) can be used for detection purpose. Signals representing $x(t)$, $y_1(t)$ and $s_1(t)$ are represented in Figs. 3(a), (b), (d), where

$$x(t) = a(t)\cos(\theta(t))$$
$$a(t) = 1 + 0.6\cos(t\pi/100)$$
$$\theta(t) = \cos(t\pi/5 + 4\sin(3t\pi/200))$$
$$y_1(t) = \sum_{k=1}^{15} f(t)\delta(t - k\alpha)$$
$$s_1(t) = x(t) + y_1(t)$$
$$s_2(t) = s_1(t) + \text{Noise}$$
$$y_2(t) = y_1(t) + \text{Noise}, \quad (35)$$

Table 1. Estimated T_B value versus SNR signals $s_1(t)$ and $s_2(t)$ using Ψ_B

Ψ_B	SNR = −6 dB	SNR = −2 dB	SNR = 1 dB	SNR = 3 dB	SNR = 5 dB	SNR = 9 dB
$(s_1(t), r_1(t))$	300 ± 1	300 ± 1	300	300	300	300
$(s_2(t), r_2(t))$	300 ± 2	300 ± 1	300 ± 1	300 ± 1	300 ± 1	300

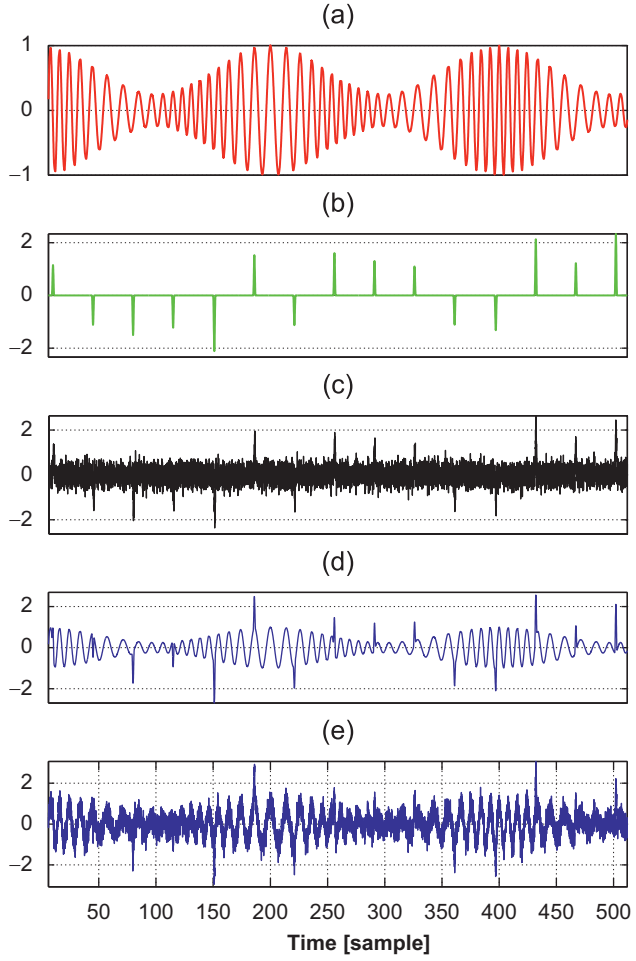

Fig. 3. Synthetic signal: (a) AM–FM signal $x(t)$. (b) Noiseless transient signal $y_1(t)$. (c) Noisy transient signal $y_2(t)$. (d) Noiseless recorded signal $s_1(t)$. (e) Noisy recorded signal $s_2(t)$.

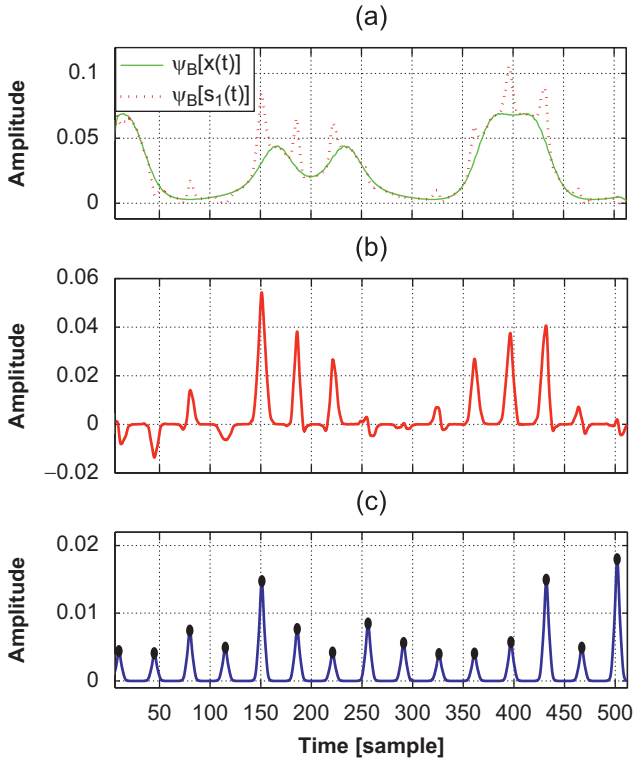

Fig. 4. Application of Ψ_B to noiseless transient detection. (a) Ψ_B output of $x(t)$ and $s_1(t)$. (b) $d_1(t) = \Psi_B(s_1(t)) - \Psi_B(x(t))$. (c) Error function $e_1(t) = \Psi_B(s_1(t) - x(t))$.

where $t \in \{1, 2, \ldots, 512\}$ and $\alpha = 32$. Coefficients $f(t)$ are independent zero mean Gaussian random numbers with variance set to 1. Signal $y_2(t)$ (Fig. 3(c)) is corrupted version of $y_1(t)$ (Fig. 3(b)) by a zero mean additive white Gaussian noise with variance set to 0.9. Signal $s_2(t)$, noisy version of $s_1(t)$, is shown in Fig. 3(e). Ψ_B is calculated using Eq. (7). Fig. 4(a) shows that over the time $\Psi_B(x(t))$ is mainly equal to $a^2(t)\omega^2(t)$ and that $\Psi_B(x(t)) \approx \Psi_B(s_1(t))$,when no pulses are detected. When $s_1(t) \neq x(t)$ $(y_1(t) \neq 0)$ the difference $d_1(t) = \Psi_B(s_1(t)) - \Psi_B(x(t))$ is different from zero where pulses are detected (Fig. 4(b)). This is confirmed by the error function $e_1(t)$ (Fig. 4(c)) where the signal, $y_1(t)$, is well detected with good time resolution compared to the signal depicted by Fig. 3(b). The detected peaks, given by $e_1(t)$, are denoted by dots.

In spite of its interest, the previous example does not account for the presence of noise component. In such case, we apply a preprocessing consisting in filtering $s_2(t)$, which leads to the filtered signal $s_f(t) = h(t) \star s_2(t)$, where $h(t)$ is the impulse response of a band-pass filter. As an example of such filter, one can use Gabor filter. In this study, this filter is set around the frequency bandwidth of $x(t)$, $(h(t) = e^{-t^2 b^2} \cos(\omega_0 t)$, $\omega_0 = \pi/5$ and $b = 0.1875)$. In general, Gabor filter is chosen for its optimal time–frequency discriminability [11]. Thus, $\Psi_B(s_f)$ is calculated using Eq. (29). Results of filtered signal, $s_f(t)$, are shown in Fig. 5. As in Fig. 4(a), when $y_2(t)$ is different from zero (Fig. 5(a)) $d_2(t) = \Psi_B(s_f(t)) - \Psi_B(x(t))$ is also different from zero (Fig. 5(b)) and clicks are well detected. The detected peaks, given by $e_2(t)$, are denoted by asterisks

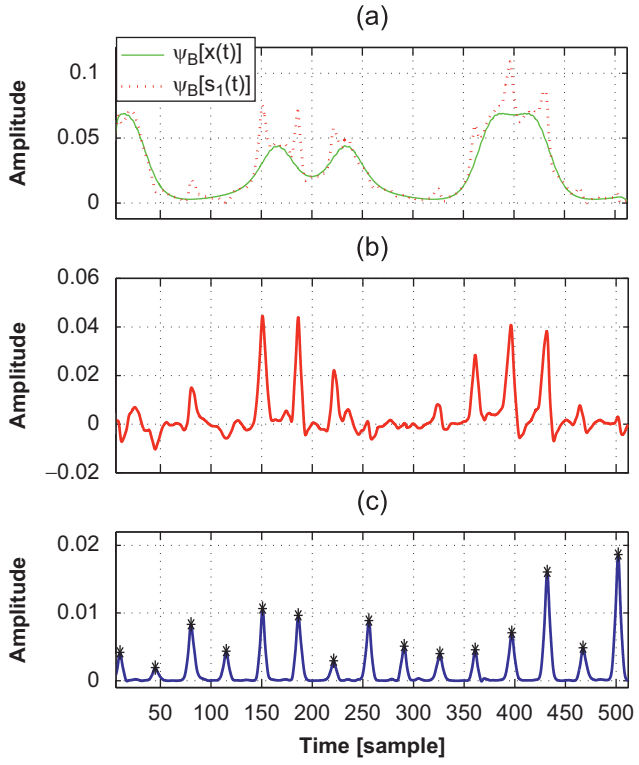

Fig. 5. Application of Ψ_B to noisy transient detection. (a) Ψ_B output of $x(t)$ and $s_f(t)$. (b) $d_2(t) = \Psi_B(s_f(t)) - \Psi_B(x(t))$. (c) Error function $e_2(t) = \Psi_B(s_f(t) - x(t))$.

(Fig. 5(c)). Results of Figs. 4(c) and 5(c), using $e_1(t)$ and $e_2(t)$, compared to those of Figs. 4(b) and 5(b), using $d_1(t)$ and $d_2(t)$, show that pulses are well detected in the former case. This is mainly due to interaction information between signals carried out by the cross-term of Eq. (34), $\Psi_B(s_i(t), x(t))$. In each case (Figs. 4 and 5) in the presence of clicks we get strong deviations of Ψ_B, even for small amplitudes of the peaks, which makes their detection easy. Furthermore, since Ψ_B uses only three time samples, $e_i(t)$ is synchronized with the transient pulse signal.

9. Conclusion

In this paper, we have pointed out some new properties of the cross-Ψ_B-energy operator that are useful for signal processing applications. We have shown that Ψ_B is a generalization of some extensions of Teager–Kaiser operator to complex signals. We have established the link between Ψ_B operator and the Lie bracket, which confirms that Ψ_B is a measure of cross-energy between two signals. Expression of Ψ_B associated with analytic signals is proposed. We have also shown that Ψ_B operator satisfies the quadratic superposition law and thus can be used efficiently for transient signals detection. Preliminary results show that Ψ_B can be used as interaction measure and as transient signal detector. As future work, we plan to investigate other properties of Ψ_B and to apply them to real world signals.

References

[1] Kaiser JF. Some useful properties of teager's energy operators. Proc ICASSP 1993;3:149–52.
[2] Cexus JC, Boudraa AO. Link between cross-wigner distribution and cross-teager energy operator. Electron Lett 2004;40:778–80.
[3] Boudraa AO, Cexus JC, Abed-Meraim K, Saidi Z. Interaction measure of AM-FM signals by cross-ψ_b-energy operator. Proc IEEE ISSPA 2005; 775–8.
[4] Boudraa AO, Cexus JC, Zaidi H. Functional segmentation of dynamic nuclear medicine images by cross-ψ_b-energy operator. Comput Meth Prog BioMed 2006;84:146–52.
[5] Boudraa AO, Cexus JC, Abed-Meraim K. Cross-ψ_b-energy operator-based signal detection. J Acoust Soc Am 2008;123: 1–7.
[6] Boudraa A, Cexus J, Groussat M, Brunagel P. An energy-based similarity measure for time series. Adv Signal Process 2008;23:1–8.
[7] Bysted TK, Hamila R, Gabbouj M, Renfors M. Teager correlation function, In: Proceedings of IEEE Nordic Signal Processing Symposium, 1998. p. 133–6.
[8] Hamila R, Astola J, Alaya Cheikh F, Gabbouj M, Renfors M. Teager energy and the ambiguity function. IEEE Trans Signal Process 1999;47:260–2.
[9] Maragos P, Bovik AC. Image demodulation using multi-dimensional energy separation. J Opt Soc Am 1995;12: 1867–76.
[10] Maragos P, Potamianos A. Higher order differential energy operators. IEEE Signal Process Lett 1995;2:152–4.
[11] Maragos P, Kaiser JF, Quatieri T. Energy separation in signal modulations with application to speech analysis. IEEE Trans Signal Process 1993;41:3025–51.
[12] Dimitriadis D, Maragos P. Robust energy demodulation based on continuous models with application to speech recognition. In: Proceedings of the European conference on speech and communication techniques, 2003. p. 1–4.
[13] Dimitriadis D, Maragos P. Continuous energy demodulation methods and application to speech analysis. Speech Commun 2007;41:819–37.

Abdel-Ouahab Boudraa was born in Constantine, Algeria. He received the B.S. degree in Physics (Electronics Engineering) from Constantine Institute of Physics, University of Constantine, Algeria, and the Engineer degree in Electronics from Educatel (Liege, Belgium). He also received the M.S. degree in Biomedical Engineering from INSA, Lyon, the University degree in Nuclear Magnetic Resonance, the Ph.D. degree in Image Processing and the University degrees in Statistics and Modeling and in Positron Emission Tomography all from the University of Claude Bernard, Lyon 1, France. He is currently Associate Professor of Electrical Engineering at Ecole Navale, Brest, France. His current

research interests include computer vision, vector quantization, data structures and analysis, data fusion, time frequency analysis, higher-order energy operators, empirical mode decomposition, hard and fuzzy pattern recognition. Dr. Boudraa is recipient of 2003 Varian Prize awarded by the Swiss Society of Radiobiology and Medical Physics for the best published paper impacting Radiation Oncology. Dr. BOUDRAA is a Senior Member IEEE.

Salem Benramdane was born in Tizi-Ouzou, Algeria. He received the Engineering degree in Mechanical Engineering from Institut Supérieur Maritime, Algeria, and the M.S. degree in Fluid Mechanics from École Cantrale de Nantes, France. He is currently a teaching and research assistant at École Navale, Brest, France, and working towards the Ph.D. degree in Fluid Mechanics. His main research interests include hydrodynamics, turbulence and model order reduction for flow control applications using methods such as the empirical mode decomposition. He is a member of ASME.

Jean-Chritophe Cexus received his engineering degree and M.S. degree in control from l'Ecole Supérieure des Sciences Appliquées pour l'Ingénieur de Mulhouse (ESSAIM) and Ph.D. degree in Signal processing from University of Rennes 1. He is currently Research engineer with French Ministry of Defense. His research interests include time–frequency analysis, empirical mode decomposition, Radar, Sonar target recognition and neural networks.

Thierry Chonavel received the Ph.D. thesis in signal processing from ENST, Paris France, in 1992. His thesis was about trigonometric moment problems and array processing. He joined Institut Telecom (Institut Telecom) in 1993, where he is currently Professor at telecom Bretagne, Brest, France. His researches are about signal processing and communications with works in adaptive processing, Radar, and applications related to underwater acoustics (ocean tomography and seismic).